Research article

Comparative predictions of turbulent non-isothermal flow of a viscoplastic fluid with yield stress

M.A. Pakhomov [a], U.K. Zhapbasbayev [b],[*]

[a] *Kutateladze Institute of Thermophysics SB RAS, Novosibirsk, Russia*
[b] *Satbayev University, Almaty, Kazakhstan*

A B S T R A C T

RANS simulation of turbulent non-isothermal flow in a pipe by transition of Newtonian fluid into a viscoplastic non-Newtonian fluid is carried out. Carrier phase turbulence was modeled using two-equation isotropic $k-\widetilde{\varepsilon}$ – model and Reynolds stress transport model. Results of calculations of Newtonian and non-Newtonian power-law fluids were compared with data of DNS calculations of other authors. Comparisons with data from other works for isothermal Schwedoff-Bingham fluid were performed in this work using $k-\widetilde{\varepsilon}$ – model. Satisfactory agreement was obtained with data from other studies for the axial averaged velocity and turbulent kinetic energy radial profiles (the difference is up to 15 %). Reynolds stress transport model showed significant anisotropy between streamwise and transverse velocity fluctuations (up to several times) and good agreement with DNS results of other authors. Averaged and pulsation profiles express the indicated transformation of the non-isothermal turbulent flow.

1. Introduction

Turbulent non-isothermal flows of non-Newtonian viscoplastic fluids (paraffinic oil) in pipes are of great practical importance because they are found in many industrial devices (pipelines, offshore oil transport, petroleum product, etc.). Paraffinic oil (waste crude oil) exhibits a viscoplastic property with yield point and a sharp increase in viscosity as its temperature decreases [1].

Early studies of viscoplastic fluid flows were carried out using friction coefficient correlations [2,3]. Authors have developed a methodology for predicting the coefficient of friction of power-law (PL) fluids. Later their found were used in Refs. [4–6] for study of NNF with yield stress. Authors [7,8] found friction coefficient correlations in laminar and turbulent flows using modern physical approaches [9,10]. There are large discrepancies between predictions and experiments, even when correlations have been confirmed experimentally [2,11–13]. Difference between measurements and predictions of viscoplastic fluids can be attributed to complicity and limitations of measurements in rheological fluids, for example, slurries [14] and slurry suspensions [15]. The most widely used fluid with polymer additive is Carbopol [16]. The dominant characteristics of Carbopol are yield stress and shear thinning and it is considered as an ideal viscoplastic fluid in experiments [17].

Direct numerical simulation (DNS) is the most accurate and powerful modern method to simulate of generalized NF fluid. Schwedoff-Bingham (SB) or Herschel-Bulkley (HB) models of non-Newtonian fluids, are difficult for DNS calculations due to singular viscosity at zero shear rate [18]. The friction coefficient values obtained from DNS calculations for PL fluid in Ref. [19] agree well with

---

Nomenclature

Latin

$C_f = 2\tau_W/U_1^2$	wall friction coefficient
C_P	heat capacity
D	pipe I.D.
k	turbulent kinetic energy
L	pipe length
Nu	hD/λ_W Nusselt number
Re	$U_{m1}D/\nu_{W1}$ Reynolds number
T	temperature
T_1	temperature at the inlet
T_{W1}	inner wall temperature
U_{m1}	initial average-mass flow velocity
$\langle \mathbf{u}'t' \rangle$	turbulent heat flux
$\langle \mathbf{u}'\mathbf{u}' \rangle$	Reynolds stress
u^*	friction velocity
x, r	axial and radial coordinates
y	distance normal from the wall

Subscripts

1	initial condition
$+$	wall unit
T	turbulent parameter
W	wall
m	average-mass
S	soil

Greek

$\dot{\gamma}$	strain rate tensor
ε	dissipation of the turbulent kinetic energy
μ	molecular viscosity
μ_{eff}	effective (apparent) molecular viscosity
μ_P	is the plastic viscosity, and
λ t	hermal conductivity
ρ	density
ν	kinematic viscosity
τ_0	is the yield shear stress
τ	shear stress

Acronyms

SB	Schwedoff-Bingham
FD	fully developed Newtonian fluid
HL	Hwang and Lin
NF	Newtonian fluid
NNF	non-Newtonian fluid
PL	power-law
RANS	Reynolds-averaged Navier-Stokes equations
RSM	Reynolds stress model
TKE	turbulent kinetic energy

the measurements of [11]. It is also possible to obtain turbulence parameters, which are difficult to measure, from DNS calculations. Authors [19] also analyzed the effect of Reynolds number in turbulent flow regime on reduction of shear stresses. The turbulent kinetic energy balances are given for the power-law fluid in tube, where shear thinning is determined by a decrease in the power index n ($0 < n < 1$) [20]. The effect of power-law index n on Reynolds stresses is revealed near-wall region, where the velocity gradients as well as the shear rate fluctuations are larger. Authors of [18–21] using DNS obtained that shear-thinning effects play a large role in turbulence of carrier fluid flow. Decreasing the degree n for Herschel-Bulkley fluids can cause an increase in velocity ripples and a small decrease in Reynolds stresses. The study [22] is remarkable in that viscoelasticity was included in laminar regime using modification of the Kelvin-Voigt defining SB equation without using regularization.

The high computational cost of the DNS model for simulation of turbulent viscoplastic flows makes the RANS + RSM approach the

viable alternative for engineering applications. For the flow of viscoplastic Schwedoff-Bingham and Herschel-Bulkley fluids of RANS model are given in Refs. [23–28]. A new turbulence model based on k-ω SST model to predict turbulent flows of HB, SB and power-law fluids is presented in Ref. [29]. In this paper, the approach [27] to describe PL fluid is used to simulate Herschel-Bulkley fluid. The authors [29] believe that this approach can be employed to modeling of generalized NF. Most studies of non-Newtonian turbulent fluids focus on isothermal flow regime, while calculations of non-isothermal turbulent flows are very limited. A few papers concerned the study of heat transfer in turbulent NNF [30,31]. Turbulent viscoelastic polymer flow has been numerically predicted in Ref. [30]. The DNS study of laminar Rayleigh–Bénard convection was performed in Ref. [31].

In our work we consider axisymmetrical RANS modeling of turbulent non-isothermal flow with yield stress of a viscoplastic SB fluid. Carrier fluid turbulence is modeled using isotropic two-parametric k-$\widetilde{\varepsilon}$ – model, and Reynolds stress transport model (RSM). This model shows better results than the k-$\widetilde{\varepsilon}$ turbulence isotropic model. The novelty of the study is the transformation of the turbulent NF into viscoplastic state due to heat transfer with surrounding medium (cold soil). The results of numerical calculations for Herschel-Bulkley fluid are also given in comparison with data of other authors.

2. Model of mass and heat transfer

2.1. Rheology of a viscoplastic fluid

The effective (apparent) molecular viscosity of viscoplastic fluid can be written as [18,29]:

$$\mu_{eff} = \begin{cases} \dfrac{\tau_0}{\dot{\gamma}} + k_v \dot{\gamma}^{n-1}, \text{if } |\tau| > \tau_0 \infty, \text{if } |\tau| \le \tau_0 \,. \end{cases} \tag{1}$$

Here τ_0 is the yield stress, $|\tau| = \sqrt{\tau_{ij}\tau_{ij}}$ is stress tensor, n and k_v are rheological model parameters, $\dot{\gamma} = \sqrt{2S_{ij}S_{ij}} = S^2$ is shear rate, $S_{ij} = 0.5\left(\frac{\partial U_i}{\partial x_j} + \frac{\partial U_j}{\partial x_i}\right)$ is shear rate tensor. Expression (1) corresponds to model of Herschel-Bulkley fluid. This model reduces to SB fluid at $n = 1$, $k_v = \mu_p$ or power-law fluid at $\tau_0 = 0$. Effective viscosity demonstrates a singular property at shear stress is less than τ_0 [32] and it can be given as a smooth function [32]:

$$\mu_{eff} = \frac{\tau_0[1 - exp(-m|\dot{\gamma}|)] + k_v|\dot{\gamma}|^n}{|\dot{\gamma}|}, \tag{2}$$

where $m = 1000$ is the regularization parameter [32]. formula (2) allows solving numerical problems in the presence of yield stress for a Schwedoff-Bingham and Herschel-Bulkley fluids.

2.2. Governing equations

The equation system for turbulent non-isothermal flow of viscoplastic NNF fluid is written in Ref. [33]:

$$\nabla \cdot \mathbf{U} = 0 \tag{3}$$

$$\nabla \cdot (\rho \mathbf{UU}) = -\nabla P + \nabla \cdot (2\mu_{eff}\mathbf{S}) + \nabla \cdot \left(-\rho\langle \mathbf{u}'\mathbf{u}'\rangle\right) + \nabla \cdot \langle 2\mu'_{eff}\mathbf{S}'\rangle \tag{4}$$

$$\nabla \cdot (\rho C_p T\mathbf{U}) = \nabla \cdot (\lambda\nabla T) + \nabla \cdot \left(-\rho C_p\langle \mathbf{u}'t'\rangle\right) + \tau : \mathbf{S} \tag{5}$$

Here, **S** is averaged strain rate tensor, $S = \sqrt{2S_{ij}S_{ij}}$. The turbulent Reynolds stress $-\rho\langle \mathbf{u}'\mathbf{u}'\rangle$ are modeled using k-$\widetilde{\varepsilon}$ turbulence isotropic model and RSM approach. Turbulent heat flux $-\rho C_p\langle \mathbf{u}'t'\rangle$ is given in Ref. [33]. The expression $\nabla \cdot \langle 2\mu'_{eff}\mathbf{S}'\rangle$ in equation (4) is found according to representation [27]. The last term in equation (5) takes into account the dissipation of kinetic energy and has the form [33–35]. The expression for the average shear rate in the non-Newtonian fluid was given in Ref. [27]. Let us the average value of the molecular viscosity is related to the average value of shear rate such as the same rheological relationship as for instantaneous quantities (1) [27]. Finally, formula for the averaged shear rate can be written as [27]:

$$\langle\dot{\gamma}\rangle^2 = 2\langle S_{ij}\rangle\langle S_{ij}\rangle + (\rho\varepsilon)\big/\langle\mu\rangle, \text{ where } \langle\mu\rangle = \frac{\tau_0}{\langle\dot{\gamma}\rangle} + k_v\langle\dot{\gamma}\rangle^{n-1}\,.$$

The elliptical relaxation RSM [37] describes the nonisotropy of complex turbulent flows. This model is more complex than the k-$\widetilde{\varepsilon}$ turbulence model and shows better results for anisotropic flows. The system of basic equations of the second-moment closure model of [37] is given:

$$\frac{D\overline{u_i u_j}}{Dt} = P_{ij} + D^{\nu}_{ij} + \Phi^*_{ij} - \varepsilon_{ij} + \frac{\partial}{\partial x_l}\left(\frac{C_\mu T_T}{\sigma_k}\overline{u_l u_m}\frac{\partial\overline{u_i u_j}}{\partial x_m}\right) \tag{6}$$

$$\frac{D\varepsilon}{Dt} = \frac{C_{\varepsilon_1}P - C_{\varepsilon_2}\varepsilon}{T_T} + \frac{\partial}{\partial x_l}\left(\frac{C_\mu}{\sigma_\varepsilon}\overline{u_l u_m}\frac{\partial\varepsilon}{\partial x_m}\right) + \nu\frac{\partial^2\varepsilon}{\partial x_k \partial x_k} + C_{\varepsilon_3}\nu\frac{k}{\varepsilon}\overline{u_j u_k}\left(\frac{\partial^2 U_i}{\partial x_j \partial x_l}\right)\left(\frac{\partial^2 U_i}{\partial x_k \partial x_l}\right) \tag{7}$$

$$\chi - L_T^2 \nabla^2 \chi = 1\big/(\varepsilon T_T) \tag{8}$$

$$\Phi_{ij}^* = (1 - k\chi)\Phi_{ij}^w + k\chi\Phi_{ij}^h \tag{9}$$

$$\varepsilon_{ij} = (1 - Ak\chi)\frac{\overline{u_i u_j}}{k}\varepsilon + Ak\chi\frac{2}{3}\varepsilon\delta_{ij} \tag{10}$$

$$A = 1 - \frac{9}{8}\left(a_{ij}a_{ij} - a_{ij}a_{jk}a_{ki}\right); \; a_{ij} = \frac{\overline{u_i u_j}}{k} - \frac{2}{3}\delta_{ij} \tag{11}$$

$$\Phi_{ij}^h = -\left(g_1 + g_1^*\frac{P}{\varepsilon}\right)\varepsilon b_{ij} + g_2\varepsilon\left(b_{ik}b_{kj} - \frac{1}{3}b_{kl}b_{kl}\delta_{ij}\right) + \left(g_3 - g_3^*\sqrt{b_{kl}b_{kl}}\right)kS_{ij} +$$
$$g_4 k\left(b_{ik}S_{jk} + b_{jk}S_{ik} - \frac{2}{3}b_{lm}S_{lm}\delta_{ij}\right) + g_5 k\left(b_{ik}\Omega_{jk} + b_{jk}\Omega_{ik}\right) \tag{12}$$

$$b_{ij} = \frac{\overline{u_i u_j}}{2k} - \frac{1}{3}\delta_{ij}; \Omega_{ij} = \frac{1}{2}\left(\frac{\partial U_i}{\partial x_j} - \frac{\partial U_j}{\partial x_i}\right) \tag{13}$$

$$\Phi_{ij}^w = -5\frac{\varepsilon}{k}\left(\overline{u_i u_k}n_j n_k + \overline{u_j u_k}n_i n_k - \frac{1}{2}\overline{u_k u_l}n_k n_l\left(n_i n_j - \delta_{ij}\right)\right) \tag{14}$$

$$\overrightarrow{n} = \frac{\nabla\chi}{\|\nabla\chi\|}; \; T_T = \max\left(\frac{k}{\varepsilon}, C_T\left(\frac{\nu}{\varepsilon}\right)^{1/2}\right); \; L_T = C_L\max\left(\frac{k^{3/2}}{\varepsilon}, C_\eta\frac{\nu^{3/4}}{\varepsilon^{1/4}}\right) \tag{15}$$

where P_{ij} determines the transfer of energy from the average speed to the pulsating one;

$P = 0.5P_{kk}$; T_T expresses the macroscale of turbulent time; D_{ij}^ν determines viscous diffusion; Φ_{ij}^* determines the redistribution term; ε_{ij} determines the dissipation; ε expresses the rate of dissipation. The constants and functions of the system of equation (6)–(15) are taken from Ref. [37]. The RSM and $k - \widetilde{\varepsilon}$ models did not have additional sink and/or source terms that determine the influence of the non-Newtonian fluid on the carrier phase turbulence.

2.3. Boundary conditions

The flow schematic is shown in Fig. 1. The boundary conditions on the wall surface ($r = R = D/2$), in inlet section ($x = 0$) and at outlet edge ($x = L$) were given in details in Refs. [28,33].

On the inner surface wall ($r = R = D/2$):

$$r = R; \; U = V = k = \widetilde{\varepsilon} = 0; \; -\lambda_w\left(\frac{\partial T}{\partial r}\right)_w = \alpha_1(T_m - T_w); \; \overline{u_i u_j} = 0; \; \varepsilon = 2\nu\frac{k}{y^2}; \; \chi = 0 \tag{16}$$

On the pipe axis.

$$r = 0; \; \frac{\partial U}{\partial r} = \frac{\partial T}{\partial r} = \frac{\partial k}{\partial r} = \frac{\partial\widetilde{\varepsilon}}{\partial r} = V = 0; \; \frac{\partial\overline{u_i u_j}}{\partial r} = \frac{\partial\varepsilon}{\partial r} = \frac{\partial\chi}{\partial r} = 0 \tag{17}$$

Effect of fluid temperature on rheological properties of viscosity μ_p and yield stress τ_0 are given [28]. In Table 1 are given the values of the yield shear stress τ_0, plastic viscosity μ_P, and Bingham number $Bm = \tau_0 R/(\mu_P U_{m1})$ vs fluid temperature.
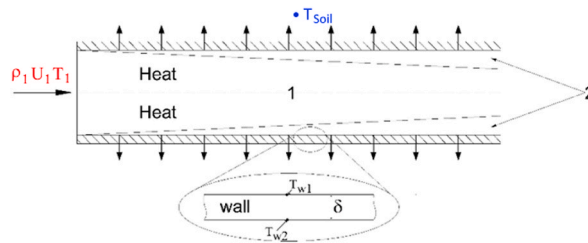

Fig. 1. Scheme of non-isothermal flow of paraffinic oil in a pipe: *1* – Newtonian fluid flow area; *2* – area of flow of the Schwedoff-Bingham non-Newtonian fluid.

Table 1
Values of yield shear stress, plastic viscosity and Bingham numbers vs fluid temperature of NNF.

t, ^0C	T, K	τ_0, Pa	μ_P, Pa·s	Bm
0	273	589.6	0.3585	822.32
5	278	34.62044	0.14634	118.29
10	283	2.03286	0.05974	17.01
15	288	0.11937	0.02438	2.45
20	293	0.00701	0.00995	0.35
25	298	4.1156E-4	0.00406	0.05
30	303	2.41662E-5	0.00166	0.007

3. Numerical realization

Numerical calculations are performed using the "in-house" code [28,33]. The set of Eq. (1–17) is solved numerically using finite control volume method, QUICK and SIMPLEC algorithms. The simulations use a non-uniform mesh (in streamwise and transverse directions) with refinement close to pipe wall and in entrance zone. The numerical realization is given in details in Refs. [28,33]. The grid convergence test (GCT) for the radial profiles of TKE is performed on the grids: 500×40 ("coarse"), 1000×80 ("basic") and 1500×120 ("fine") (see Fig. 2). The difference between "basic" and "fine" grids is very small (up to 0.1 %) and the grid with 1000×80 CVs is used in authors' simulations as the basic grid.

4. Calculation results and discussion

4.1. The $k - \widetilde{\varepsilon}$ – model of Hwang and Lin (HL) verification for the isothermal Newtonian fluid

The predicted results of the wall friction coefficient C_f obtained using the $k - \widetilde{\varepsilon}$ – model [36] and RSM [37] are presented in Table 2 at various Reynolds numbers for turbulent air flow in a round pipe. Table 2 also shows the result of the calculation using the Blasius formula [38]: $C_f = 0.0791 \text{Re}^{-1/4}$. The data in Table 2 shows the calculations by the $k - \widetilde{\varepsilon}$ – model [36] and RSM [37] model agree well with the Blasius theoretical formula given in Ref. [38].

The results of the comparative analysis with DNS data and PIV and LDA experiments [39] are shown in Fig. 3 according to the radial distributions of the average axial velocity (a), turbulent kinetic energy (TKE) (b) and the rate of its dissipation (c). DNS results and measurements [39] were carried out at $\text{Re} = U_c 2R/\nu = 7000$; $\text{Re}_\tau = u^* 2R/\nu = 360$; $x/(2R) = 75$; $2R = 95$ mm, where U_c is centerline fluid velocity. Calculation by HL model satisfactorily agrees with the data [39] on the axial velocity distributions. The predicted position of the peak of the turbulence at $r/R = 0.91$ using the HL [36] and RSM [37] models according well to the DNS [39]. The characteristic value of the maximum is $k^+ = k/u_*^2 \approx 4.4$ according to the data of [39], which is greater than $k^+ \approx 3.75$ according to the calculations using the model [36] (the difference is up 18 %). Also, HL model gives satisfactory agreement with the data [39] on the dissipation rate of TKE for almost the entire pipe section (the difference does not exceed 15 %). The DNS shape of profile of dissipation of TKE also agrees qualitatively and quantitative with the calculation by the model [36]. The difference is increased in near-wall region at $r/R \geq 0.975$. The value of dissipation rate of TKE predicted by the HL model close to the wall is $\varepsilon^+ = \varepsilon/\nu u_*^4 \approx 0.12$. Whereas
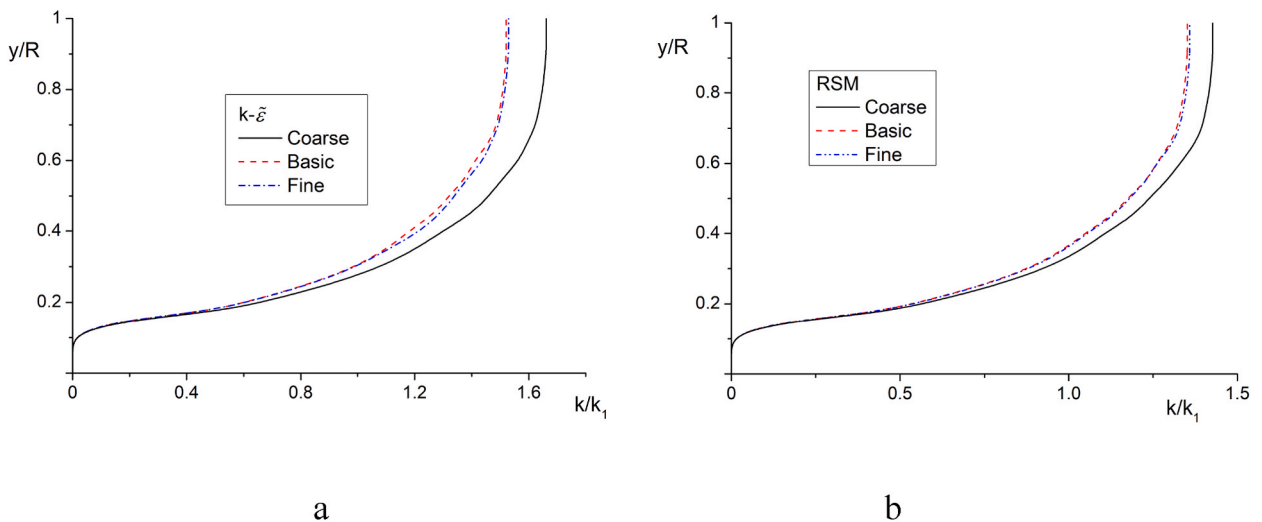

a   b

Fig. 2. The grid convergence test for the $k - \widetilde{\varepsilon}$ (a) and (b) RSM models of in-house numerical code. $L = 2$ m, Re $= 8200$, $U_1 = 0.2$ m/s, $T_1 = 298$ K, $T_W = 273$ K.

Table 2
Calculation of the coefficient of wall friction vs the Reynolds numbers.

C_f	HL [36]	RSM [37]	Blasius [38]
Re = 5000	0.009	0.0092	0.0094
1.34×10^4	0.0071	0.00725	0.00735
3.2×10^4	0.0056	0.006	0.00591
10^5	0.0042	0.0046	0.00445

a

b

c
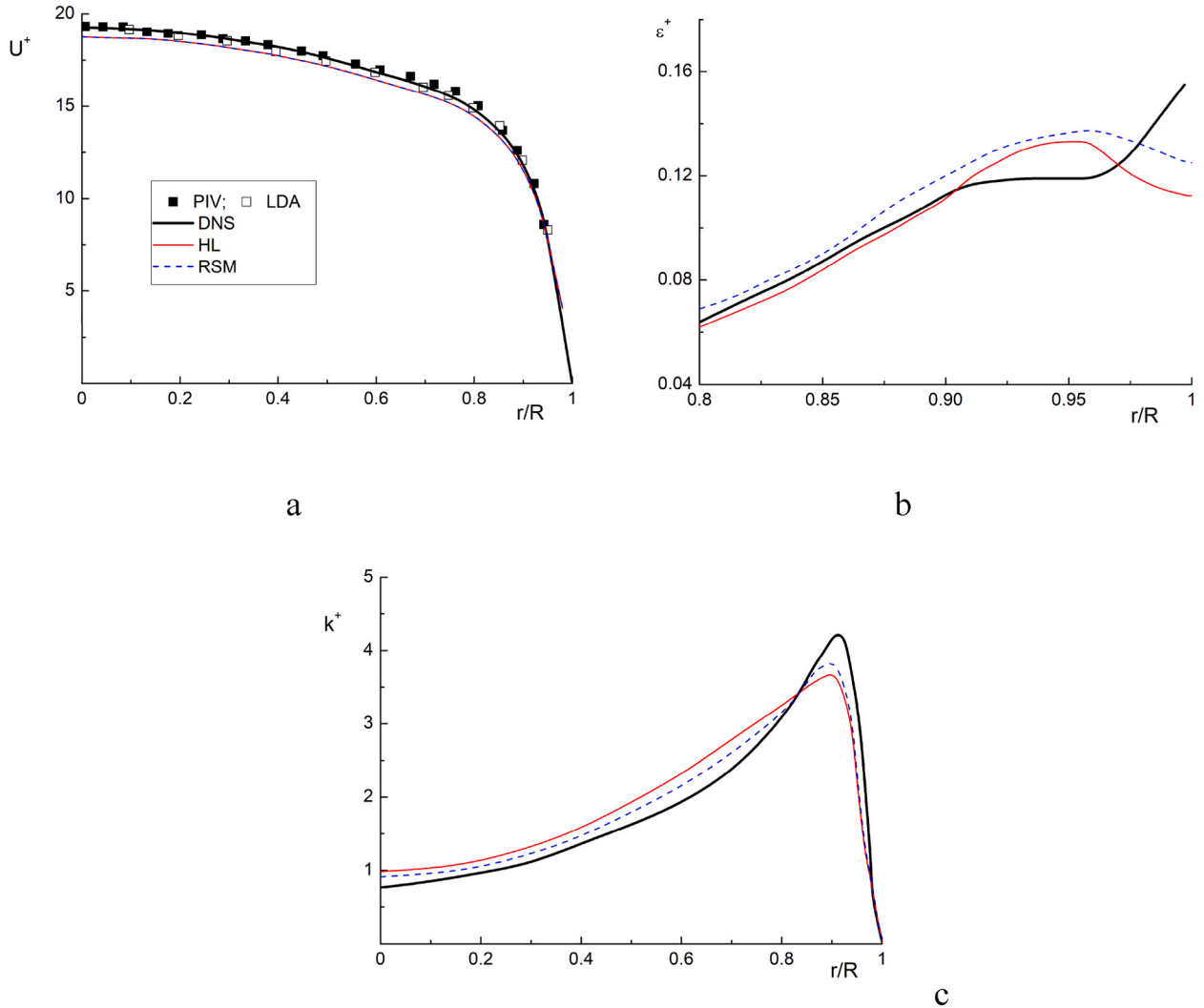
Fig. 3. Comparisons between the DNS (bold lines), LDA (open points) and PIV (closed points) experimental data of [39] and authors' results: HL [36] (solid lines) and RSM [37] (dashed lines).

according to DNS data [39] $\varepsilon^+ \approx 0.16$ (the difference is up to 33 %). The overwhelming majority of two-parametric turbulence models cannot accurately predict the profile of dissipation rate of TKE near the wall [39].

4.2. Averaged and turbulent characteristics of a power-law isothermal fluid

For the comparative analysis we used RANS numerical calculations [27] and DNS [18,40] for PL fluid flow in a pipe at variation of power in parameter n and different Reynolds numbers of flow. In this case, the model for calculating average viscosity of turbulent NNF corresponds to that [27,40]. In this comparison, the RANS data [27] were used, where only the influence of average viscosity was taken into account and no additional terms in the turbulence model for non-Newtonian fluid were taken into account. Results of DNS calculations [21] were used when performing comparison of results for the Schwedoff-Bingham fluid. All authors' numerical results are

presented in Figs. 4–6 were obtained using the RANS and RSM turbulence model.

Figs. 4 and 5 shows comparative results of the distribution of average axial velocity $U^+ = U/u_*$ (a), turbulent kinetic energy (TKE) $k^+ = k/u_*^2$ (b) and Reynolds stress $\langle uv \rangle^+ = \langle uv \rangle/u_*^2$ (c) as a function distance from the pipe wall $y^+ = \mu u_* y/\mu_W = \mu u_* (R-r)/\mu_W$. Where μ is the molecular viscosity of a Newtonian fluid (waxy crude oil). Reynolds stresses were calculated from the dependence of $\langle u_i u_j \rangle = -\nu_T \left(\frac{\partial U_i}{\partial x_j} + \frac{\partial U_j}{\partial x_i} \right) + \frac{2}{3} k \delta_{ij}$ (for $k - \widetilde{\varepsilon}$ – model). The authors' RANS + RSM calculations have been carried out for the PL fluid at $n = 0.6$ and the NF ($n = 1$) in Figs. 4 and 5 at Reynolds number Re $= 0.75 \times 10^3$ and 10^4, respectively. The dots are data of DNS calculations [18,40], the lines are numerical RANS calculations [27] and authors' RANS + RSM. Additionally, Figs. 4a and 5a show logarithmic velocity profile for Newtonian fluid (bold lines).

Characteristic axial velocity profiles in laminar sublayer correspond to linear wall law for both Newtonian and power-law fluids (see Figs. 4a and 5a). Also note that values of average velocities of power-law and Newtonian fluids are practically the same in this part of the pipe. Good agreement of authors' calculations for non-Newtonian power-law fluid with the results [18,27,40] for laminar sublayer is obtained. Further, at $y^+ > 9$, deviation from linear profile for non-Newtonian fluid is obtained. In logarithmic layer according to RANS calculations of [27] and authors we got exceeding of axial flow speed value in comparison with DNS results [18,40] for non-Newtonian liquid (max difference is less than 20 %). Also for power-law fluids noticeable deviation from logarithmic velocity profile is shown, reaching 35 %. The above features are characteristic both for our calculations and for the data [18,27,40] in the whole range of investigated variation of flow Reynolds number.

Figs. 4b and 5b show the distribution of turbulent kinetic energy (TKE) across the pipe cross section. The turbulence level in the power-law fluid k^+ is higher than the corresponding value for the Newtonian fluid across the pipe cross section for our calculations for both Reynolds number values. The maximum additional generation of turbulence level in non-Newtonian fluid reaches 15 %. Note that this conclusion is not in agreement with RANS calculations [27], which show suppression of TKE level (see Fig. 2b), but qualitatively
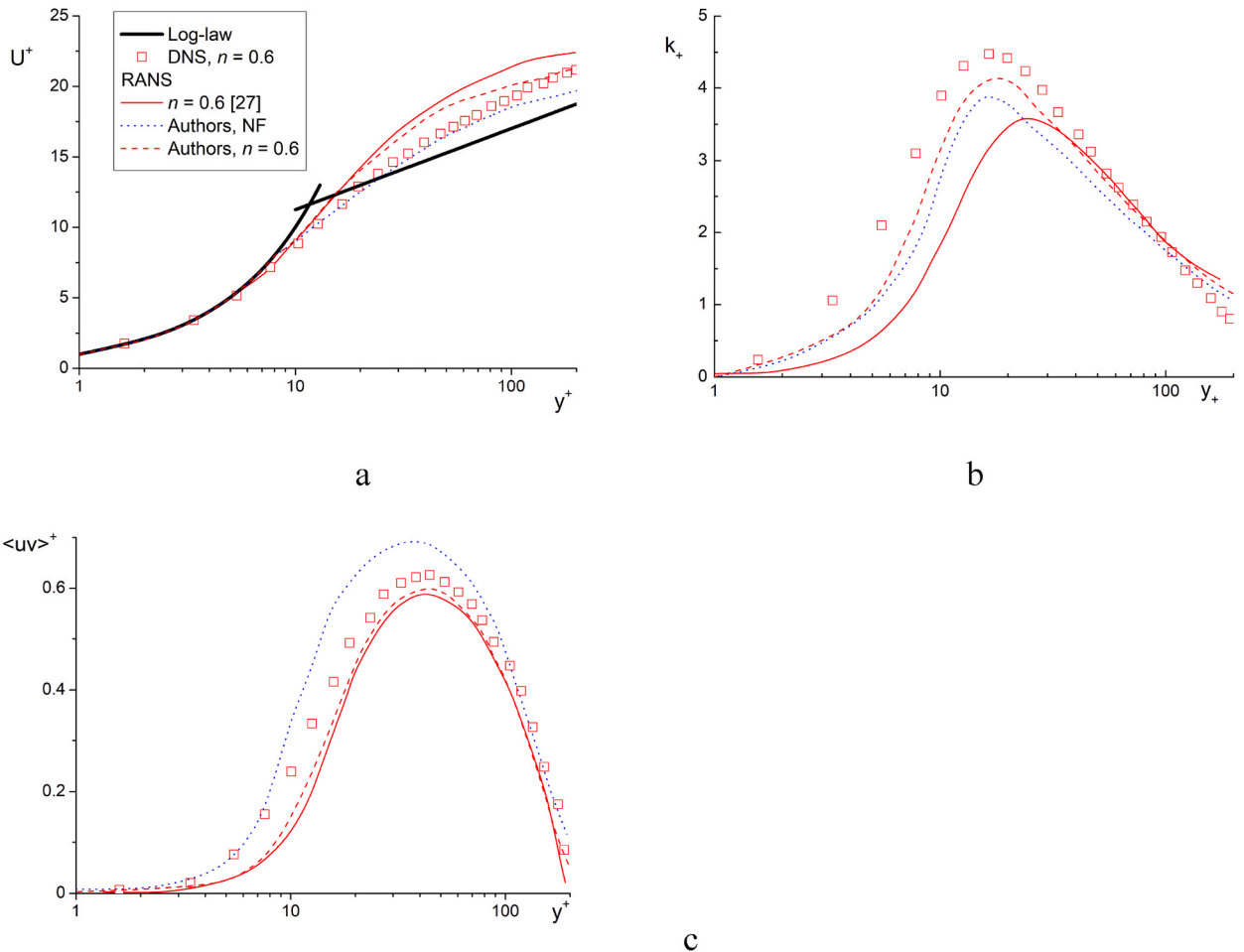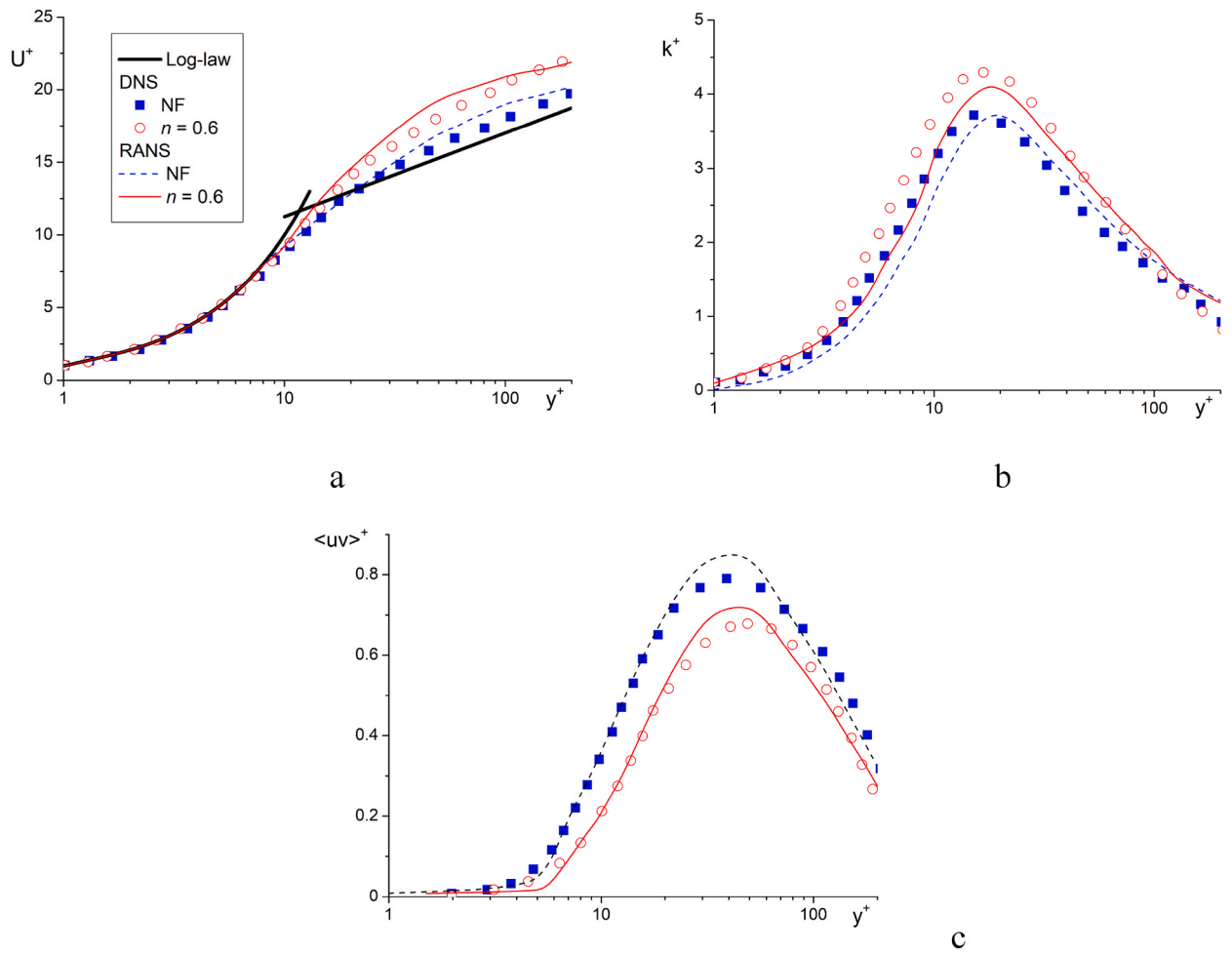

Fig. 4. Comparison of the dimensionless axial velocity (a), turbulence kinetic energy (b), and Reynolds stresses (c) in wall coordinates for Newtonian and power-law fluids. Bold lines in Fig. 4a are logarithmic velocity profile, symbols are DNS at $n = 0.6$ [18]. Solid lines are RANS calculations at $n = 0.6$ (power-law fluid) [27]; dotted and dashed lines are authors' RANS + RSM calculations at $n = 1$ (Newtonian fluid) and 0.6 (power-law fluid), respectively. Re $= U_m D/\mu_W = 0.75 \times 10^4$, Re$_\tau = u_* D/\mu_W = 210$.

Fig. 5. Comparison of the dimensionless axial velocity (a), turbulence kinetic energy (b), and Reynolds stresses (c) in wall coordinates for Newtonian and power-law fluids. Bold lines in Fig. 5a are logarithmic velocity profile, solid and open symbols are DNS [40] for $n = 1$ (NF) and 0.6 (power-law) fluids, respectively; dashed and solid lines are the authors' RANS + RSM simulations for the NF and $n = 0.6$ (power-law fluid), respectively. $Re = 10^4$, $Re_\tau = 310$.
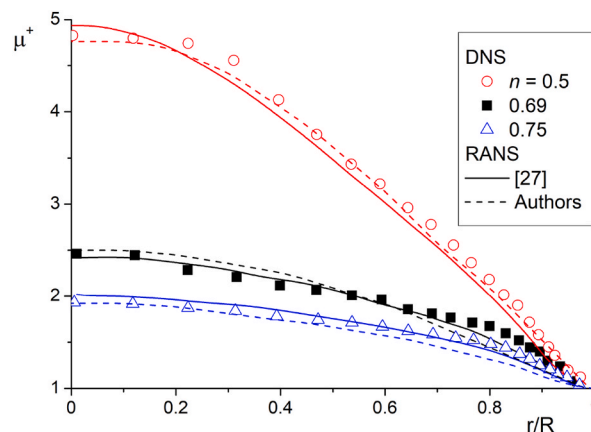

Fig. 6. Comparisons of the dimensionless average viscosity of a power-law fluid. Symbols are the DNS [18], solid and dashed lines are RANS calculations [27] and authors' RANS + RSM, respectively. $Re = 0.55 \times 10^4$, $Re_\tau = 160$. $1 - n = 0.5$, $2 - 0.69$, $3 - 0.75$.

corresponds to DNS results [18,40]. In the laminar layer, the largest discrepancy with the DNS data is obtained and reaches 50 %. In the logarithmic layer ($y^+ = 10–100$) the difference between DNS and our calculation data does not exceed 15 %. Then it increases again and at $y^+ = 200$ is about 50 %. It was shown in Refs. [18,40] that in non-Newtonian fluid axial fluctuations are higher than that ones in Newtonian fluid, while radial and tangential fluctuations are lower. This is explained by the fact that in a non-Newtonian fluid, due to pressure fluctuations, the mechanism of energy transfer from axial fluctuations to the other two components is suppressed [21]. For these DNS calculations [18,40] at $y^+ > 120$ an insignificant decrease of turbulence level (up to 5 %) in a power-law fluid in comparison with Newtonian flow is obtained. In our work, as in Refs. [18,27,40], the generation of turbulence in a non-Newtonian fluid in comparison with a Newtonian fluid is shown.

Reynolds shear stresses $\langle uv \rangle^+$ in PL fluid are lower than that one for NF (see Figs. 4c and 5c). The position of their maximum is shifted towards the pipe axis (not more than 10 %) in the power stage power-law fluid compared to the Newtonian medium. This quantitatively agrees well with RANS [27] and DNS [18,40] (maximum difference less than 10 %).

The profiles of the average viscosity of a power-law fluid $\mu^+ = \mu/\mu_W$ across cross section of pipe are shown in Fig. 6. Here μ and μ_W are values of the viscosity of non-Newtonian fluid at the considered point and at the pipe wall respectively. A satisfactory agreement between our calculation results and the DNS [18] and RANS [27] simulations of turbulent power-law non-Newtonian fluids at Re = 5500 and power exponents $n = 0.5, 0.69$ and 0.75 is observed. The viscosity significantly increases towards pipe axis and with decreasing value of parameter n. For the value $n = 0.5$ the maximum value of the relative viscosity at the pipe axis $\mu^+ \approx 5$, and at $n = 0.75$ the maximum growth reaches two times and $\mu^+ \approx 2$. This is typical both for our DNS data and for the results of [18,40].

4.3. Averaged and turbulent characteristics of the Schwedoff-Bingham fluid

Comparison of DNS data [21] and our RANS calculations in wall coordinates for Newtonian fluid (lines *1* and *3*) and for SB turbulent fluid (curves *2–6*) is shown in Figs. 7 and 8. In Fig. 7 points are DNS data [21], lines are RANS calculation of authors [28] using $k-\tilde{\varepsilon}$ – model [36], Re = $U_{m1}D_1/\nu_{W1} = 1.3 \times 10^4$, Re$_\tau = u*R_1/\nu_W = 323$. The axial (see Fig. 7a) and radial (see Fig. 7b) velocities fluctuation profiles show differences with the DNS data [21]. The Reynolds stresses (in axial and radial directions) are typically predicted in $k-\tilde{\varepsilon}$ – model [36]: $u' = v' = 2k/3$. The axial averaged velocity profile along the tube cross section is qualitatively similar to the one for a Newtonian fluid. This is characteristic both for the DNS data [21] and for our RANS calculations. For the axial averaged velocity distributions, it is possible to note an excess by RANS calculations (up to 10 %) in comparison with DNS [21]. Distributions of TKE calculated by author's agree satisfactorily well with the DNS [21] and difference is up to 15 %. These data are given in Ref. [28] and are not presented here in order to reduce the manuscript volume. However, the isotropic $k-\tilde{\varepsilon}$ – model [36] does not even qualitatively describe the complex distribution of velocity fluctuations over the pipe cross section and significant anisotropy of axial and radial velocity fluctuations of SB fluid.

Therefore, authors' RANS and $k-\tilde{\varepsilon}$ – model [36] predicted axial and radial velocities fluctuations (solid lines) of fluid are the same for NF and NNF. Turbulence model of [36] captures the main effect of non-Newtonian behavior on fluid turbulence and difference between NF and NNF is obvious. Fig. 7a and b clearly show the deficiency of isotropic turbulence models. In our simulations well-known isotropic distributions of axial and radial velocity pulsations is used: $u' = v' = 2k/3$. Difference between DNS [21] and our results obtained using $k-\tilde{\varepsilon}$ – model for axial velocity fluctuations is up to 20 % and it is reasonable quantitative difference. The main discrepancy is revealed for the radial velocity fluctuations (up to 3 times). It is seen the $k-\tilde{\varepsilon}$ – model is predicted the radial component in a reasonable way, but the quantitative difference is large. The locus of maximal radial velocity fluctuations for DNS [21] is located at
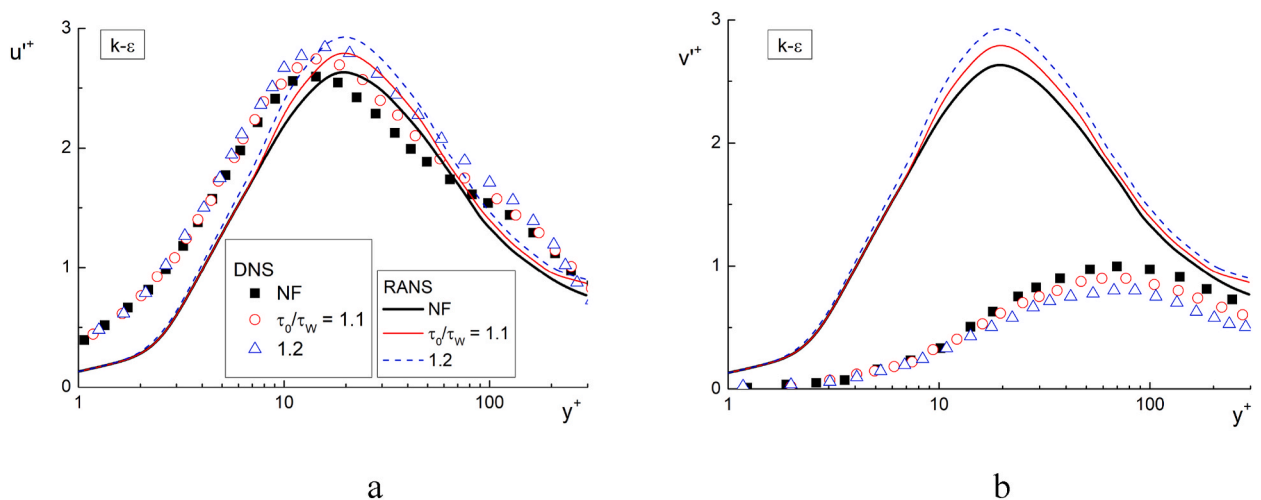

Fig. 7. Comparisons of the results of authors' RANS calculations using the $k-\tilde{\varepsilon}$ – model [36] of axial $u'^+ = u'/u_*$ (a) and radial $v'^+ = v'/u_*$ (b) velocity fluctuations of the Schwedoff-Bingham fluid with the DNS results [21]. Symbols are DNS [21], lines are authors' RANS calculations using the $k-\tilde{\varepsilon}$ – model [36].
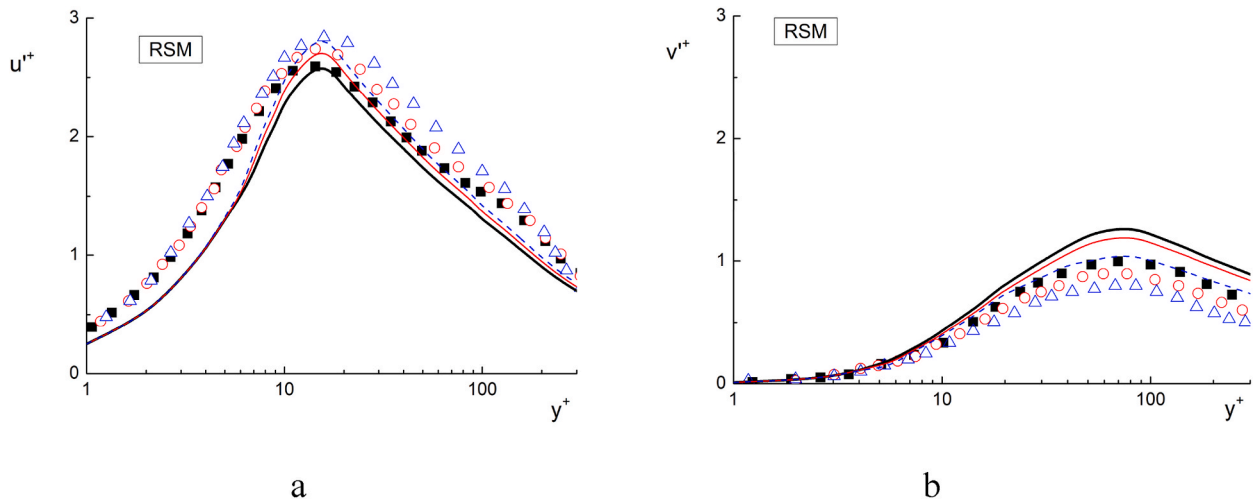
Fig. 8. Comparisons of the results of authors' RANS calculations using the RSM model [37] of axial $u'^+ = u'/u_*$ (a) and radial $v'^+ = v'/u_*$ (b) velocity fluctuations of the Schwedoff-Bingham fluid with the DNS results [21]. The legends to the figures are the same as in Fig. 7.

$y^+ \approx 70$ and it locates for the $k-\widetilde{\varepsilon}$ − model [36] at $y^+ \approx 20$. In reality, streamwise and transverse fluid velocity fluctuations are not the same. This is demonstrated by DNS simulations [21]. The difference between axial and radial fluid velocity fluctuations obtained using DNS reaches almost 3 times (see Fig. 7a and b).

For the Schwedoff-Bingham fluid the results of the RSM model calculations of the axial $u'^+ = u'/u_*$ (a) and radial $v'^+ = v'/u_*$ (b) velocity fluctuation profiles are shown in Fig. 8. Here points are DNS [21], lines are RANS calculation of authors using RSM model [37]. As can be seen from the data shown in Fig. 8, the RSM model qualitatively well describes the anisotropy of the axial and radial velocity fluctuation profiles. The positions of maximum values and practically coincide with DNS data [21]. The obtained calculation data confirm the possibility of successful use of the RSM model [37] to describe non-isothermal flow of the SB fluid. Further in our calculations of flow and heat transfer at transition of turbulent NF to NNF we will use exactly RSM model [37].

The following crucial points can be noted in conclusion to these two subsections concerning the verification a numerical model for describing turbulent isothermal power-law and Schwedoff-Bingham fluids. The use of the isotropic $k-\widetilde{\varepsilon}$ − model [36] makes it possible to predict, in the first approximation, the distributions of the averaged parameters of the turbulent flow (averaged axial velocity and TKE) of non-Newtonian fluids with a reasonable degree of accuracy. However, this model is completely unsuitable for calculating axial and radial components of carrier phase velocity fluctuations (up to 300 %). The use of RSM of [37] in describing turbulence makes it possible to calculate the anisotropic behavior of turbulent characteristics in axial and radial directions of non-Newtonian fluids with satisfactory accuracy (up to 20 %).

4.4. Predictions of turbulent non-isothermal flow structure

Fig. 1 shows a diagram of the flow of non-isothermal waxy crude oil (WCO) in an underground oil pipeline. The Reynolds number is Re$=U_1 D/\nu_{W1} = (0.4$–$1.2) \times 10^4$ and Prandtl number Pr $= \mu_{W1} C_{P1}/\lambda_1 = 42$. The pipe has an inner diameter D $= 2R = 0.2$ m and a length L = 20 m (x/D = 100). A turbulent flow of a Newtonian fluid flows into the pipe entrance. Then WCO cools down by flowing along pipe length due to heat transfer through pipe wall with cold soil. Reynolds number is based on the fluid viscosity determined under wall conditions and the viscosity depends on the fluid temperature.

Results of calculations of non-isothermal motion in the pipe show change of state of Schwedoff-Bingham fluid (paraffinic oil). The value of longitudinal velocity in core zone increases (up to 1.7 times in comparison with velocity at the inlet cross-section), and it decreases in the wall zone. As oil flows through the pipe, the height of the section with fully stopped fluid in pipe gradually increases and reaches y/R ≈ 0.15 at x/D = 20 (see Fig. 9a). Accordingly, the core area with maximum fluid velocity decreases to y/R ≈ 0.9.

Turbulent kinetic energy increases significantly in the flow core (more than 1.75 times) and noticeably decreases in the near-wall zone (see Fig. 9b). TKE for axisymmetric flow is determined by well-known equation: $2k \approx \langle u'^2 \rangle + 2\langle v'^2 \rangle$. The boundary of region of NF properties has been determined. Profiles of evolution of dimensionless temperature $\Theta = (T - T_{W1})/(T_1 - T_{W1})$ of fluid show cooling of paraffinic oil flow due to heat exchange with environment through pipe wall (see Fig. 9c). Here T_{W1} is wall temperature at the inlet section. Yield stress profiles τ_0/τ_{NF} are shown in Fig. 9d, where τ_{NF} is the shear stress value in the turbulent Newtonian fluid. The radial profiles of average dynamic viscosity coefficient distributions $\mu_{eff}/(\mu_{T1}+\mu_1)$ are given in Fig. 9e. Here μ_{eff} is the effective averaged viscosity of the turbulent NNF and $(\mu_{T1}+\mu_1)$ is the sum of turbulent and molecular viscosities of NF (waxy crude oil) at the inlet. This ratio is clearly showing of non-Newtonian behavior of the fluid movement. Decrease in fluid temperature in near-wall zone by turbulent Newtonian fluid cooling causes significant increase in the value of average dynamic viscosity coefficient of fluid.

Non-Newtonian fluid properties appears and yield shear stress τ_0 arises when a fluid temperature $T \leq 293$ K [1,41,42]. The fluid flow (WCO) exhibits the NF behavior when $T > 293$ K. This agrees with numerical calculations data for laminar flow of waxy crude oil
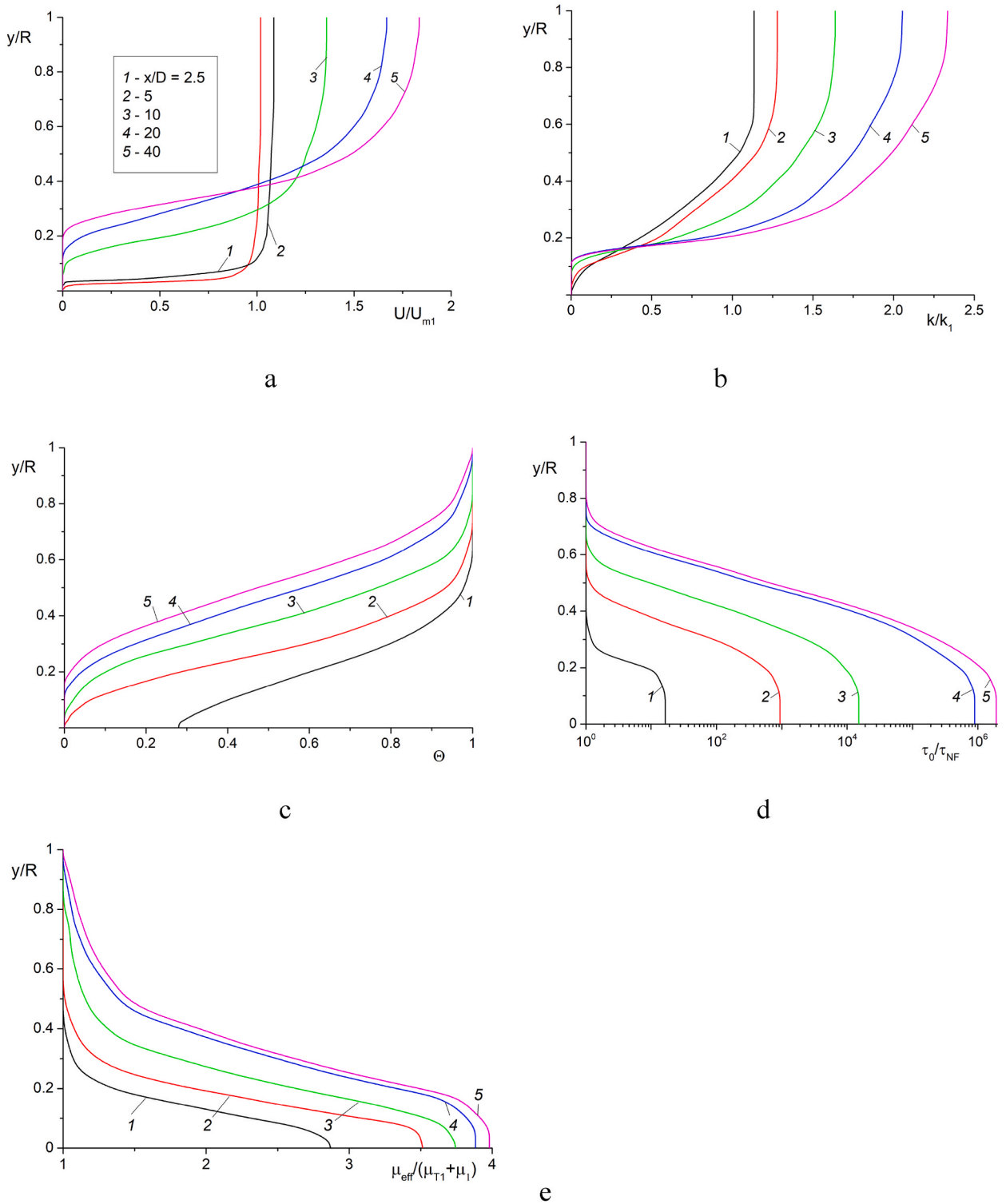
Fig. 9. Distributions of the dimensionless average axial velocity U/U_{m1} (a), turbulent kinetic energy k/k_1 (b), average temperature Θ (c) and yield shear stress τ_0/τ_{NF} (d) and averaged effective dynamic viscosity (e). $Re = 8200$, $T_1 = 298$ K, $T_S = 273$ K.

in a pipe [11]. Earlier in works [35,41,42] it was shown that heat transfer of moving fluid flow in pipe or channel and surrounding ground has the main influence on manifestation of non-Newtonian properties of SB liquid. The results of numerical calculations for influence of ambient soil temperature T_S on turbulent characteristics of paraffinic oil are shown in Fig. 10. For a Newtonian fluid, flow
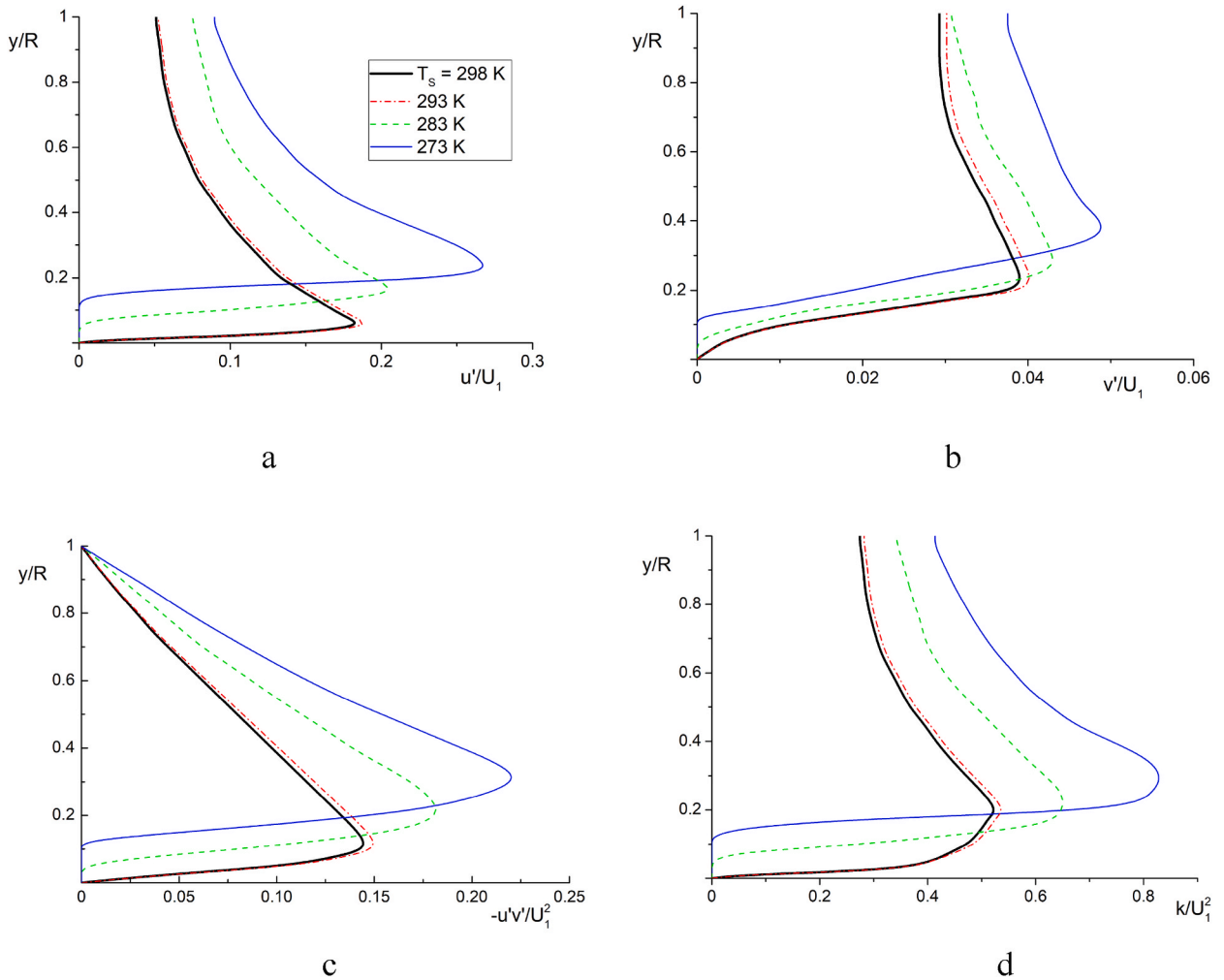
Fig. 10. Effect of soil temperature T_S on the profiles of axial u'/U_1 (a), radial v'/U_1 (b) turbulent fluctuations, Reynolds stresses $\overline{u'v'}/U_1^2$ (c) and turbulence kinetic energy k/U_1^2 (d): Re = 8200, $x/D = 20$, $T_1 = 298$ K.

and heat transfer calculations were performed for paraffinic oil without taking into account the non-Newtonian properties at $T_S = 298$ K. Note that for NF our numerical calculations are in good agreement with DNS [18]. These results are not given in these figures.

A decrease in the temperature of the surrounding soil causes the additional generation of turbulence in the flow core and its significant suppression in the near-wall part of the pipe (see Fig. 10). There is a shift of position point of turbulent pulsation level maximum, Reynolds stress and TKE towards the pipe axis. In Newtonian liquid it is located $y/R \approx 0.1$ for axial fluctuations, Reynolds stress and TKE (see Fig. 10). For a liquid with manifestation of non-Newtonian properties and ultimate shear stress ($T_S = 273$ K), the maximum is located at ($y/R \approx 0.23$). The ratio of axial velocity fluctuations to radial fluctuations one is AR= $(u'/v')_{max} \approx 5.3$ and shows significant turbulence anisotropy (see Fig. 10).

The appearance and behavior of the non-Newtonian viscoplastic properties in waxy crude oil is given in Fig. 11. The ratio of τ_0/τ_{NF} = 10 is used as the threshold value of appearance of NNF viscoplastic behavior. Height y_0 is the distance from the wall where the yield stress magnitude of $\tau_0 = 10\tau_{NF}$ and τ_{NF} is the shear stress value in the turbulent Newtonian fluid. Let us assume when this ratio of τ_0/τ_{NF} is reached, the flow becomes completely viscoplastic. The height of near-wall part of the pipe with lowered temperature increases towards pipe core zone due to fluid cooling and correspondingly the length of NNF manifestation zone increases. Height of non-Newtonian behavior zone increases as the Reynolds number of flow (velocity) decreases.

The temperature of the carrier fluid is reduced due to the heat exchange of waxy crude oil with the environment. This causes an increase in plastic viscosity and a yield stress in the near-wall zone of the pipe. The values of plastic viscosity and yield stress in the near-wall region increase for a colder carrier fluid. As temperature decreases, length of near-wall zone of the viscoplastic fluid expands, covering more and more parts of the pipe. Figs. 9–11 clearly demonstrate the occurrence of a stagnation zone and the viscoplastic state of the fluid, and also illustrate the transition of paraffinic oil from the Newtonian state to the viscoplastic Schwedoff-Bingham state due to heat transfer with cold environment.
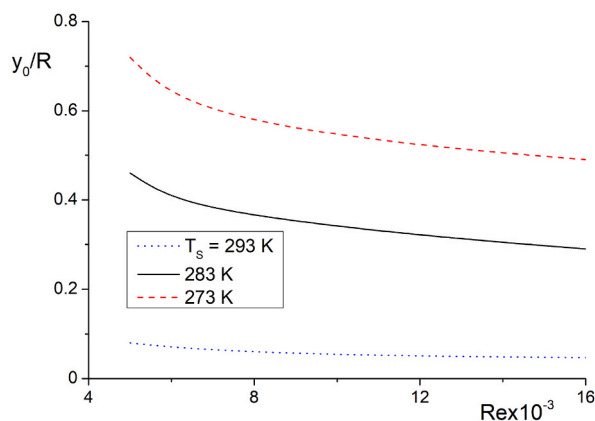
Fig. 11. The effect of Reynolds numbers on the distance from the wall with the yield stress appearance in SB fluid at $x/D = 20$.

5. Conclusion

A numerical study of flow motion and heat transfer of a turbulent non-isothermal Schwedoff-Bingham fluid in a pipe has been carried out. The calculated data show the transition of an incompressible Newtonian fluid to a non-Newtonian viscoplastic fluid flow. A better agreement with the DNS calculations on distribution of turbulent non-Newtonian flow characteristics is obtained by including additional sink and source terms in the transport equations for the averaged flow characteristics. It should be noted axial velocity of Schwedoff-Bingham and power-law non-Newtonian fluids in logarithmic part of the pipe flow larger than that one in the case of Newtonian flow.

One of the significant results is an increase of turbulent kinetic energy in flow core and damping in zone of yield stress manifestation. A numerical result obtained with Reynolds stress model qualitatively describes the anisotropy of axial and radial velocity fluctuations well. The locations of maximum values of axial and radial velocity fluctuations are in agreement with DNS of other authors.

Additional information

No additional information is available for this paper.

CRediT authorship contribution statement

M.A. Pakhomov: Methodology, Conceptualization. **U.K. Zhapbasbayev:** Methodology, Conceptualization.

Declaration of competing interest

The authors declare that they have no known competing financial interests or personal relationships that could have appeared to influence the work reported in this paper.

Acknowledgements

References

[1] U.K. Zhapbasbayev, G.I. Ramazanova, D.Zh Bossinov, B.K. Kenzhaliyev, Flow and heat exchange calculation of waxy oil in the industrial pipeline, Case Stud. Therm. Eng. 26 (2021) 101007.
[2] A.B. Metzner, J.C. Reed, Flow of nonnewtonian fluids-correlation of the laminar, transition, and turbulent-flow regions, AIChE J. 1 (4) (1955) 434–440.
[3] D.W. Dodge, A.B. Metzner, Turbulent flow of non-Newtonian system, AIChE J. 5 (2) (1959) 189–204.
[4] D.J. Guillot, J.H. Denis, Prediction of laminar and turbulent friction pressures of cement slurries in pipes and centered annuli, in: European Petroleum Conference, Society of Petroleum Engineers, SPE-18377-MS, 1988.
[5] T.D. Reed, A.A. Pilehvari, A new model for laminar, transitional, and turbulent flow of drilling muds, in: SPE Production Operations Symposium, Society of Petroleum Engineers, SPE-25456-MS, 1993.
[6] K. Founargiotakis, V.C. Kelessidis, R. Maglione, Laminar, transitional and turbulent flow of Herschel-Bulkley fluids in concentric annulus, Can. J. Chem. Eng. 86 (4) (2008) 676–683.
[7] H.R. Anbarlooei, D.O.A. Cruz, F. Ramos, C.M.M. Santos, A.P. Freire Silva, Phenomenological friction equation for turbulent flow of Bingham fluids, Phys. Rev. E 96 (2) (2017) 023107.

[8] H.R. Anbarlooei, D.O.A. Cruz, F. Ramos, C.M.M. Santos, A.P. Freire Silva, On the connection between Kolmogorov microscales and friction in pipe flows of viscoplastic fluids, Physica D 376 (2018) 69–77.

[9] S.B. Pope, Turbulent Flows, Cambridge University Press, Cambridge, 2000.

[10] G. Gioia, P. Chakraborty, Turbulent friction in rough pipes and the energy spectrum of the phenomenological theory, Phys. Rev. Lett. 96 (4) (2006) 044502.

[11] M.P. Escudier, F. Presti, Pipe flow of a thixotropic liquid, J. Non-Newtonian Fluid Mech. 62 (2–3) (1996) 291–306.

[12] F. Presti, Investigation of Transitional and Turbulent Pipe Flow of Non-newtonian Fluids, Ph.D. thesis, University of Liverpool, 2000.

[13] J. Peixinho, C. Nouar, C. Desaubry, B. Théron, Laminar transitional and turbulent flow of yield stress fluid in a pipe, J. Non-Newtonian Fluid Mech. 128 (2–3) (2005) 172–184.

[14] V.C. Kelessidis, P. Dalamarinis, R. Maglione, Experimental study and predictions of pressure losses of fluids modeled as Herschel-Bulkley in concentric and eccentric annuli in laminar, transitional and turbulent flows, J. Petrol. Sci. Eng. 77 (3–4) (2011) 305–312.

[15] A. Nikbakht, A. Madani, J.A. Olson, D.M. Martinez, Fibre suspensions in Hagen– Poiseuille flow: transition from laminar plug flow to turbulence, J. Non-Newtonian Fluid Mech. 212 (2014) 28–35.

[16] M. Dinkgreve, M. Fazilati, M.M. Denn, D. Bonn, Carbopol: from a simple to a thixotropic yield stress fluid, J. Rheol. 62 (3) (2018) 773–780.

[17] R.S. Mitishita, J.A. MacKenzie, G.J. Elfring, I.A. Frigaard, Fully turbulent flows of viscoplastic fluids in a rectangular duct, J. Non-Newtonian Fluid Mech. 293 (2021) 104570.

[18] M. Rudman, H.M. Blackburn, L.J.W. Graham, L. Pullum, Turbulent pipe flow of shear-thinning fluids, J. Non-Newtonian Fluid Mech. 118 (1) (2004) 33–48.

[19] J. Singh, M. Rudman, H.M. Blackburn, Reynolds number effects in pipe flow turbulence of generalized Newtonian fluids, Phys. Rev. Fluids 3 (9) (2018) 094607.

[20] J. Singh, M. Rudman, H.M. Blackburn, The influence of shear-dependent rheology on turbulent pipe flow, J. Fluid Mech. 822 (2017) 848–879.

[21] J. Singh, M. Rudman, H.M. Blackburn, The effect of yield stress on pipe flow turbulence for generalised Newtonian fluids, J. Non-Newtonian Fluid Mech. 249 (2017) 53–62.

[22] M.E. Rosti, D. Izbassarov, O. Tammisola, S. Hormozi, L. Brandt, Turbulent channel flow of an elastoviscoplastic fluid, J. Fluid Mech. 853 (2018) 488–514.

[23] M.R. Malin, The turbulent flow of Bingham plastic fluids in smooth circular tubes, Int. Commun. Heat Mass Tran. 24 (6) (1997) 793–804.

[24] M.R. Malin, Turbulent pipe flow of Herschel-Bulkley fluids, Int. Commun. Heat Mass Tran. 25 (3) (1998) 321–330.

[25] A. Bartosik, Modelling of a turbulent flow using the Herschel–Bulkley rheological model, Chem. Process Eng. 27 (1) (2006) 623–632.

[26] A. Bartosik, Application of rheological models in prediction of turbulent slurry flow, Flow, Turbul. Combust. 84 (2) (2010) 277–293.

[27] A.A. Gavrilov, V.Y. Rudyak, Reynolds-averaged modeling of turbulent flows of power-law fluids, J. Non-Newtonian Fluid Mech. 227 (2016) 45–55.

[28] M.A. Pakhomov, U.K. Zhapbasbayev, RANS modeling of turbulent flow and heat transfer of non-Newtonian viscoplastic fluid in a pipe, Case Stud. Therm. Eng. 28 (2021) 101455.

[29] S. Lovato, G.H. Keetels, S.L. Toxopeus, J.W. Settels, An eddy-viscosity model for turbulent flows of Herschel–Bulkley fluids, J. Non-Newtonian Fluid Mech. 301 (2022) 104729.

[30] M. Masoudian, F.T. Pinho, K. Kim, R. Sureshkumar, A RANS model for heat transfer reduction in viscoelastic turbulent flow, Int. J. Heat Mass Tran. 100 (2016) 332–346.

[31] S. Yigit, J. Hasslberger, N. Chakraborty, M. Klein, Effects of Rayleigh-Bénard convection on spectra of viscoplastic fluids, Int. J. Heat Mass Tran. 147 (2020) 118947.

[32] T.C. Papanastasiou, Flows of materials with yield, J. Rheol. (N. Y., NY, U. S.) 31 (5) (1987) 385–404.

[33] M.A. Pakhomov, U.K. Zhapbasbayev, D.Zh Bossinov, Numerical simulation of the transition of a Newtonian to a viscoplastic state in a turbulent flow, J. King Saud Univ. Sci. 35 (2) (2023) 102522.

[34] G. Vinay, A. Wachs, J.-A. Agassant, Numerical simulation of non-isothermal viscoplastic waxy crude oil flows, J. Non-Newtonian Fluid Mech. 128 (2–3) (2005) 144–162.

[35] T.T. Bekibayev, D.Zh Bossinov, U.K. Zhapbasbayev, A.D. Kudaibergen, G.I. Ramazanova, Mismatch problem of the model and topology of oil pumping facilities, Complex Use of Mineral Resources 326 (3) (2023) 16–24.

[36] C.B. Hwang, C.A. Lin, Improved low-Reynolds-number $k-\varepsilon$ – model based on direct simulation data, AIAA J. 36 (1) (1998) 38–43.

[37] R. Manceau, K. Hanjalic, Elliptic blending model: a new near-wall Reynolds-stress turbulence closure, Phys. Fluids 14 (2) (2002) 744–754.

[38] H. Schlichting, K. Gersten, Boundary-Layer Theory, Springer Verlag, Berlin, 2000.

[39] J.G.M. Eggels, F. Unger, M.H. Weiss, J. Westerweel, R.J. Adrian, R. Friedrich, F.T.M. Nieuwstadt, Fully developed pipe flow: a comparison between direct numerical simulation and experiment, J. Fluid Mech. 268 (1994) 175–209.

[40] A.A. Gavrilov, V.Y. Rudyak, Direct numerical simulation of the turbulent flows of power-law fluids in a circular pipe, Thermophys. Aeromechanics 23 (4) (2016) 473–486.

[41] G.T. Chala, S.A. Sulaiman, A. Japper-Jaafar, A. Flow start-up and transportation of waxy crude oil in pipelines-A review, J. Non-Newtonian Fluid Mech. 251 (2018) 69–87.

[42] J. Zhao, W.Q. Zhao, S.L. Chi, Y.W. Zhu, H. Don, Quantitative effects of different factors on the thermal characteristics of waxy crude oil pipeline during its shutdown, Case Stud. Therm. Eng. 19 (2020) 100615.